Structural and biochemical basis of FANCI-FANCD2 interdependent ubiquitination

Kimon Lemonidis*, Martin L. Rennie, Connor Arkinson, Viduth K. Chaugule, Mairi Clarke, James Streetley, Helen Walden*

*Corresponding Authors

Abstract

The Fanconi Anaemia pathway operates for the repair of interstrand crosslinks and the maintenance of genomic stability upon replication stalling. Di-monoubiquitination of the FANCI-FANCD2 (ID2) complex is a central and crucial step in this pathway. Evidence suggests that FANCD2 ubiquitination precedes FANCI ubiquitination, and that both the FANCD2-ubiquitinated ($ID2_{Ub}$) and the di-monoubiquitinated ($I_{Ub}D2_{Ub}$) complex clamp on DNA. However, FANCD2 is deubiquitinated at a faster rate than FANCI, which can result in a FANCI-ubiquitinated ID2 complex ($I_{Ub}D2$). Here, we present a 4.1 Å cryo-EM structure of $I_{Ub}D2$ complex bound to double-stranded DNA. We show that this complex, like $ID2_{Ub}$ and $I_{Ub}D2_{Ub}$, is also in the closed ID2 conformation and clamps on DNA. While the target lysine of FANCD2 (K561) is partially buried in the non-ubiquitinated ID2-DNA complex, it becomes fully exposed in the $I_{Ub}D2$-DNA structure, and thus can be ubiquitinated at a faster rate. The $I_{Ub}D2$-DNA complex cannot easily revert to the non-ubiquitinated ID2 state, due to USP1-UAF1-resistance, conferred by the presence of DNA and FANCD2. $ID2_{Ub}$-DNA, on the other hand, can be efficiently deubiquitinated by USP1-UAF1, unless further ubiquitination on FANCI occurs. FANCI ubiquitination also progresses at a faster rate in $ID2_{Ub}$-DNA over ID2-DNA complex, and results in partial DNA-dependent protection from FANCD2 deubiquitination. Taken together, our results suggest that, while FANCD2 ubiquitination promotes FANCI ubiquitination, FANCI ubiquitination in turn maintains FANCD2 ubiquitination by two mechanisms: it prevents excessive FANCD2 deubiquitination within an $I_{Ub}D2_{Ub}$-DNA complex, and it enables re-ubiquitination of FANCD2 within a transient, closed-on-DNA, $I_{Ub}D2$ complex.

Introduction

The Fanconi anaemia (FA) pathway is responsible for repairing interstrand crosslinks (ICLs) and ensuring that genome stability is maintained when replication is stalled (Nalepa & Clapp, 2018). A crucial and central step in this pathway is the mono-ubiquitination of FANCD2 and FANCI on specific lysines (K561 and K523 respectively for human proteins) catalysed by a multi-component ubiquitin ligase (FA-core complex) and the UBE2T ubiquitin-conjugating enzyme (Lemonidis *et al*, 2021). The two ubiquitination events are interdependent, since mutation on either of the two lysines results in greatly impaired in-cell ubiquitination on the other lysine (Smogorzewska *et al*, 2007). Removal of the two ubiquitins, through isopeptide cleavage by the USP1-UAF1 complex, is also required for ICL repair and maintenance of genomic stability (Oestergaard *et al*, 2007; Kim *et al*, 2009; Murai *et al*, 2011). Several biochemical data (Sato *et al*, 2012; Longerich *et al*, 2014; Rajendra *et al*, 2014; Chaugule *et al*, 2019; Rennie *et al*, 2020) and recent structural evidence (Wang *et al*, 2021) indicate that FANCD2 is

the preferred substrate for ubiquitination and that FANCI ubiquitination likely occurs once FANCD2 has been ubiquitinated. Upon binding to the FA-core-UBE2T, the FANCI-FANCD2 (ID2) complex closes on DNA, and this ID2 remodelling exposes and brings K561 of FANCD2 in proximity to UBE2T's catalytic cysteine for ubiquitination (Wang *et al*, 2021). The ID2 closure on DNA is maintained upon FANCD2 ubiquitination (Alcón *et al*, 2020; Wang *et al*, 2020; Rennie *et al*, 2020). The resulting $ID2_{Ub}$-DNA complex can be susceptible to USP1-UAF1-mediated deubiquitination. However, further ID2 ubiquitination on FANCI results in enhanced protection of FANCD2's ubiquitin from USP1-UAF1 action (Rennie *et al*, 2020). Moreover, FANCI appears to be even more resistant to de-ubiquitination than FANCD2, in this DNA-bound di-monoubiquitinated ($I_{Ub}D2_{Ub}$-DNA) state (Rennie *et al*, 2020; van Twest *et al*, 2017; Wang *et al*, 2020). Hence, the preferential targeting of FANCD2 for deubiquitination, is likely to result in an ID2 complex that is ubiquitinated on FANCI-only ($I_{Ub}D2$). Currently, we have no information on: i) what conformation such a complex adopts, ii) how does it bind to DNA, iii) how well it supports FANCD2-ubiquitination and iv) how efficiently $I_{Ub}D2$ is protected from deubiquitination. Providing an answer to such questions would greatly enhance our understanding on how the interdependency in FANCI-FANCD2 *in vivo* ubiquitination (Smogorzewska *et al*, 2007) is encoded at the molecular level, and elucidate the mechanism by which FANCI and FANCD2 ubiquitination are linked.

In this work, we show that a transient $I_{Ub}D2$-DNA complex is most likely formed due to significantly faster rate of FANCD2 over FANCI deubiquitination. We further demonstrate that FANCI ubiquitination maintains the closed-on-DNA ID2 conformation when FANCD2 ubiquitination is lost. We lastly show that, in this conformation, FANCD2 ubiquitination is favoured, while FANCI deubiquitination is restricted. Similar to $I_{Ub}D2$-DNA complex having a propensity to transform into an $I_{Ub}D2_{Ub}$-DNA complex, the $ID2_{Ub}$-DNA complex also has the propensity to give rise to a di-mono-ubiquitinated complex: this is achieved due to ID2 displaying significantly faster kinetics of FANCI ubiquitination upon FANCD2 ubiquitination. Hence, our results indicate that ubiquitination of either ID2 subunit results in an ID2-DNA clamp that promotes ubiquitination of the other subunit.

Results

To assess the difference between FANCD2 and FANCI deubiquitination, we assayed $I_{Ub}D2_{Ub}$ complex deubiquitination by USP1-UAF1 in a time-course. We found that indeed the rate of FANCI deubiquitination progresses at a much slower rate than FANCD2 deubiquitination (Fig. 1). This suggests that an ID2 complex which is ubiquitinated only on FANCI ($I_{Ub}D2$), may derive from USP1-UAF1-mediated $I_{Ub}D2_{Ub}$ deubiquitination. Previous Protein Induced Fluorescence Enhancement (PIFE) assays in our lab showed that, while fully-ubiquitinated (or FANCD2-only-ubiquitinated) ID2 display a 10-fold increase in affinity for double-stranded DNA (dsDNA), relative to non-ubiquitinated ID2, FANCI-only-ubiquitination results in only a 3-fold enhancement in ID2-DNA affinity (Rennie *et al*, 2020). A possible interpretation for this would be that an $I_{Ub}D2$ complex has a different conformation from ID2 and $ID2_{Ub}$/$I_{Ub}D2_{Ub}$, which would allow a different mode of binding to dsDNA. We thus sought to determine the structure of such complex bound to dsDNA, to elucidate how this may differ from $ID2_{Ub}$ and $I_{Ub}D2_{Ub}$, and understand how $I_{Ub}D2$ exactly interacts with dsDNA.

To address these questions, we assembled a 1:1:1 $I_{Ub}D2$-DNA complex from purified I_{Ub}, D2 and dsDNA (61 bp long) and determined its structure by cryo-EM, at 4.14Å global resolution and a local resolution of 2.8-13.9Å (Fig. EV1A-E; Table 1). Our final $I_{Ub}D2$-DNA map was made of 139,601 image particles, while we also obtained few smaller-sized-particle 2D class averages (4 classes; 62,961 particle images in total), likely corresponding to dissociated monomeric proteins (Fig. EV2). Using the

structure of $I_{Ub}D2_{Ub}$-DNA (Wang *et al*, 2020)(PDB: 6VAE) as initial model (but with the ubiquitin conjugated to FANCD2 removed) for refinement, we obtained an atomic model of the $I_{Ub}D2$-DNA structure at 4.1Å resolution (Table 1; Fig. 2A and EV1E). Our maps had several well-resolved regions for modelling, like the one surrounding and including FANCI's K523 isopeptide linkage with G76 of ubiquitin (Fig. EV1F) and the region of FANCI-FANCD2 C-termini interaction (Fig. EV1G). Many FANCI and FANCD2 loops, as well as the FANCI N-terminus (region corresponding to the first 170 aa) had very poor density and were thus unmodelled (Fig 2A). Modelled regions of relatively poor density included the dsDNA (Fig. EV1H), the central region of FANCD2 and an N-terminal part of FANCI (Fig. EV1E). Interestingly, we found that $I_{Ub}D2$ has the same closed-on-DNA conformation as $I_{Ub}D2_{Ub}$ and $ID2_{Ub}$ (Fig. 2A). We hypothesized that the apparent lower than expected enhancement of ID2-DNA affinity upon FANCI ubiquitination measured before, may had been due to I_{Ub} dissociating from D2 at low concentrations. Indeed, previous PIFE assays showed that at lower concentrations of $I_{Ub}D2$ (<100 nM) there had been negligible protein-binding induced fluorescence enhancement of labelled DNA, while at higher protein concentrations (>500 nM), the $I_{Ub}D2$ -binding induced fluorescence enhancement of labelled DNA, had been comparable to that achieved with $I_{Ub}D2_{Ub}$ and $ID2_{Ub}$ complexes (Rennie *et al*, 2020). Hence, to ensure complex formation at low FANCI concentrations, we performed dsDNA-binding PIFE assays for ID2 and $I_{Ub}D2$ as before (Rennie *et al*, 2020), but this time we titrated only FANCI (ubiquitinated or not), while having a constant high concentration of FANCD2 - equal to the maximum concentration of FANCI used. With such set-up, our PIFE assays revealed a 20-fold increase in ID2 affinity for dsDNA when FANCI was ubiquitinated, whereas FANCD2 on its own had negligible binding to dsDNA (Fig. 2B). The above indicate that FANCI-ubiquitination is responsible for maintaining the clamping of the ID2 complex on DNA, when FANCD2 ubiquitination is lost.

The overall conformation of the $I_{Ub}D2$ complex is very similar to that of $I_{Ub}D2_{Ub}$ (Fig. EV2A). The most noticeable differences are: i) slight movements of FANCD2 and FANCI helices in the region where FANCD2's ubiquitin interacts with FANCI; and ii) the high level of disorder in the FANCI N-terminus proximal to that region (residues 1-170), upon loss of FANCD2 ubiquitination (Fig. EV2B-C).

While both $I_{Ub}D2_{Ub}$-DNA (EMD-21138) and $ID2_{Ub}$-DNA (EMD-21139) maps display relatively poor density for FANCI N-terminus (Wang *et al*, 2020), there is virtually no density for that part in both our locally-filtered and Phenix-auto-sharpened map (Fig EV1E and Fig. 3A, respectively). Lack of density in the N-terminus of FANCI has been also observed before, upon extraction of FANCD2's ubiquitin by USP1 (Rennie *et al*, 2021). We thus propose that the high level of disorder in the FANCI N-terminus is a direct consequence of the loss of binding between the ubiquitin of FANCD2 and the N-terminus of FANCI. A crucial role for the stabilization of the FANCI's N-terminus in the $I_{Ub}D2_{Ub}$-DNA complex might be FANCI's K83 interaction with E34 of ubiquitin (Fig. EV2B). Similarly, reduced density for the N-terminus of FANCD2 has been previously observed in closed state ID2 conformations in which there is no ubiquitin conjugated to FANCI, like in the $ID2_{Ub}$-DNA (EMD-21139) map (Wang *et al*, 2020) (Fig. 3A; *right*) and USP1-UAF1-$ID2_{Ub}$-DNA (EMD-11934) map (Rennie *et al*, 2021).

We reasoned that the relative disorder in the N-terminal regions of FANCI or FANCD2, in $I_{Ub}D2$-DNA or $ID2_{Ub}$-DNA complexes respectively, might be crucial for ubiquitination of FANCD2 or FANCI, correspondingly. Despite the slight movements of $I_{Ub}D2$'s FANCI and FANCD2 towards the region where FANCD2-conjugated ubiquitin would be (Fig. EV2B-C), FANCD2's K561 is fully accessible for ubiquitination, when compared to its position in the ID2-DNA complex (32% buried) (Fig. 3B). Similarly, FANCI's K523 is also fully accessible for ubiquitination in the $ID2_{Ub}$-DNA complex, in contrast to its position in the ID2-DNA complex (65% buried) (Fig. 3B). These observations led us to the hypothesis that ubiquitination of either of the two subunits of ID2 (FANCI or FANCD2) actually favours ubiquitination of the other subunit. Indeed, time-course ubiquitination assays revealed that: FANCD2

133 ubiquitination is stimulated when FANCI is already ubiquitinated; and similarly, FANCI ubiquitination
134 is stimulated when FANCD2 is already ubiquitinated (Fig. 3C). These results may partially explain the
135 *in vivo* interdependency in FANCI and FANCD2 ubiquitination observed before (Smogorzewska *et al*,
136 2007).

137 We have previously found that in the presence of dsDNA, FANCI ubiquitination (but not FANCI
138 itself) restricts FANCD2 deubiquitination (Arkinson *et al*, 2018). We wondered whether a similar
139 mechanism exists for protection of FANCI ubiquitination: i.e. the very slow FANCI deubiquitination in
140 the $I_{Ub}D2_{Ub}$-DNA complex (Fig. 1) may be due I_{Ub} being protected from USP1-UAF1-mediated
141 deubiquitination, when associating with both $D2_{Ub}$ and DNA. Alternatively, the presence of FANCD2
142 (irrespective of ubiquitination status) and/or dsDNA may hinder USP1-UAF1 from targeting FANCI's
143 ubiquitin. To test those possibilities we performed USP1-UAF1 deubiquitination assays with either
144 isolated FANCI/FANCD2 proteins (I_{Ub} or $D2_{Ub}$), or differentially ubiquitinated ID2 complexes ($I_{Ub}D2$,
145 $I_{Ub}D2_{Ub}$ or $ID2_{Ub}$), in the presence or absence of dsDNA (Fig. 4A). We observed that dsDNA significantly
146 protects against FANCI deubiquitination, whether I_{Ub} is in isolation, or in complex with $D2/D2_{Ub}$.
147 Moreover, the protective role of DNA against FANCI deubiquitination, is further enhanced when I_{Ub} is
148 in complex with FANCD2, and this enhancement was irrespective of FANCD2 ubiquitination status (Fig.
149 4A-B). This suggests that both DNA and FANCD2 are required for maximal protection of I_{Ub} against
150 USP1-UAF1 deubiquitination. In agreement with what we observed before (Arkinson *et al*, 2018;
151 Rennie *et al*, 2020), the presence of FANCI did not affect FANCD2 deubiquitination, which was nearly
152 complete in our reaction conditions, whether FANCI was present or not (Fig. 4A). However, the
153 inclusion of ubiquitinated FANCI in our reactions, restricted to some extent FANCD2 deubiquitination,
154 when DNA was also present (Fig. 4A-B).

155 Relative to FANCI, FANCD2 is efficiently deubiquitinated. This is achieved thanks to a USP1 N-
156 terminal region (proximal to its USP domain) specifically targeting FANCD2 (Arkinson *et al*, 2018).
157 Indeed, when deubiquitination occurred under same conditions, but with a USP1 having this N-
158 terminal region (first 54 amino-acids) deleted (USP1ΔN), FANCD2 deubiquitination was nearly
159 abolished, whether $D2_{Ub}$ was in isolation or in complex with I/I_{Ub}. The USP1 substitution with the
160 USP1ΔN mutant in our assays, however, did not greatly affect FANCI deubiquitination (Fig. 4C).
161 Moreover, the presence of either D2 or $D2_{Ub}$, provided I_{Ub}-deubiquitination protection from USP1ΔN-
162 UAF1 (Fig. 4C), similarly to what observed with wild-type USP1-UAF1 complex (Fig. 4A-C). The above
163 suggest that the interaction of FANCD2's ubiquitin with FANCI (in the $I_{Ub}D2_{Ub}$-DNA complex) does not
164 protect against FANCD2 deubiquitination, as the latter can be efficiently achieved by a mechanism
165 that involves USP1's N-terminus. However, the interaction of FANCI's ubiquitin with FANCD2 (in $I_{Ub}D2$-
166 DNA and $I_{Ub}D2_{Ub}$-DNA complexes) efficiently protects against FANCI deubiquitination. The ubiquitin
167 conjugated to FANCI has two major (predominantly hydrophobic) interfaces with FANCD2 in our
168 structure (Fig. 4D). Of these two interfaces, one is absent in equivalent ubiquitin-FANCI interactions in
169 $ID2_{Ub}$-DNA structure (Wang *et al*, 2020)(Fig. 4D-E). Similarly, in the $I_{Ub}D2_{Ub}$-DNA structure, only
170 FANCD2 forms such interface with the adjacent ubiquitin, whereas FANCI does not (Wang *et al*, 2020).
171 Our structure indicates that this ubiquitin-FANCD2 interface is mediated by hydrophobic interactions
172 of residues H209 (α11 helix), P44 and V243 (α13 helix) of FANCD2 with residues T9 and K11 of
173 ubiquitin, and is further stabilized by hydrogen bonding between FANCD2's H209 and S251 with
174 Ubiquitin's T9 and R74, respectively (Fig. 4C). The residues of FANCD2 predicted to be involved in this
175 interface show a high level of conservation among vertebrate species (Fig. 4F). Hence, the above
176 interactions may be crucial for the maintenance of ID2 ubiquitination (and therefore of ID2 clamping
177 on DNA) in vertebrates.

178

Discussion

ICLs and/or replication stress result in FA-core catalysed ID2 ubiquitination, which enables the ID2 complex to clamp on DNA (Lemonidis *et al*, 2021). Since ubiquitinated ID2 is able to slide on DNA *in vitro*, it has been proposed that ID2 ubiquitination effectively functions in sliding the ID2 complex away from ICLs/replication forks. This would allow nucleases or other factors to act for the repair of ICLs and/or restoration of replication, while the ID2 clamp may protect the DNA or have a processivity function (Wang *et al*, 2020). Loss of FANCD2 ubiquitination has been found to be equally bad for cell survival as loss of FANCD2, in response to the ICL-inducing agent, mitomycin C (Garcia-Higuera *et al*, 2001). In contrast, loss of FANCI ubiquitination has been shown to be less severe than loss of FANCI in similar cell-survival assays (Smogorzewska *et al*, 2007). Moreover, *in vivo* data show that blocking FANCD2 ubiquitination (K561R mutant) completely abolishes FANCI ubiquitination, whereas blocking FANCI ubiquitination (K523R mutant) greatly impairs, but does not completely abolish FANCD2 ubiquitination (Smogorzewska *et al*, 2007). Lastly, recent structural and biochemical evidence reveal that the FA-core complex and UBE2T preferentially target for ubiquitination the FANCD2 subunit of the ID2 complex, while FANCI ubiquitination lags (Wang *et al*, 2021).

The above indicate that in cells, FANCD2 ubiquitination most likely precedes FANCI ubiquitination, and because the two ubiquitination events are linked, FANCI ubiquitination is absolutely dependant on FANCD2 ubiquitination. Upon FANCD2 ubiquitination, the C-termini of FANCI and FANCD2 close around DNA and this movement is associated with exposure of FANCI's target lysine (K523) (Wang *et al*, 2020; Lemonidis *et al*, 2021). As a result, FANCI ubiquitination is greatly enhanced (Fig. 3). Indeed, and in agreement with what has been observed before with FA-core catalysed reactions (Wang *et al*, 2021), we found that, the rate of FANCI ubiquitination is significantly higher in $ID2_{Ub}$-DNA complex than in ID2-DNA complex (Fig. 3C). In the presence of DNA, FANCI ubiquitination is required for protecting FANCD2's ubiquitin from excessive deubiquitination (Fig. 4A) (Arkinson *et al*, 2018; Rennie *et al*, 2020). Albeit slower in $I_{Ub}D2_{Ub}$-DNA complex, FANCD2 deubiquitination can still progress at significantly faster rate than FANCI deubiquitination (Fig. 1). Removal of FANCD2's ubiquitin from the $I_{Ub}D2_{Ub}$-DNA complex does not impact on either the closed-on-DNA ID2 conformation (Fig. 2), or the high level protection of FANCI's ubiquitin from USP1-UAF1-mediated deubiquitination. In fact, our deubiquitination assays indicate that I_{Ub} sensitivity to USP1-UAF1 action is conferred only by the absence of DNA, while enhanced protection is achieved when both FANCD2 and DNA are present (Fig. 4A). FANCD2's target lysine (K561) is exposed for re-ubiquitination in the $I_{Ub}D2$-DNA complex (Fig. 3A-B), and indeed the rate of FANCD2 ubiquitination in that complex is significantly greater than in the ID2-DNA complex (Fig. 3C). Hence, we propose a model whereby the balance between FANCD2 ubiquitination/deubiquitination determines whether FANCI gets ubiquitinated. Once FANCI ubiquitination is established, it plays a two-fold role: it prevents excessive FANCD2 deubiquitination (in $I_{Ub}D2_{Ub}$-DNA complex), and it ensures FANCD2 re-ubiquitination (in $I_{Ub}D2$-DNA complex), once ubiquitin has been removed from FANCD2 (Fig. 5). The clamping on DNA of $I_{Ub}D2$ and $I_{Ub}D2_{Ub}$ complexes ensures that maximum protection against USP1-UAF1 activity is achieved for both conjugated ubiquitins.

The exact mechanism by which DNA is protecting both FANCD2 and FANCI from deubiquitination is yet unclear. For the protection seen on I_{Ub} in the absence of D2, there is a possibility that DNA blocks access of USP1-UAF1 to FANCI's ubiquitin, either directly or indirectly through altering the conformation of I_{Ub}. Further structural work will be required to elucidate how USP1-UAF1 targets the ubiquitin on FANCI and how DNA may interfere with such targeting. The deubiquitination protection of $I_{Ub}D2$ and $I_{Ub}D2_{Ub}$ complexes by DNA is likely mediated through stabilisation of the ubiquitinated ID2 complexes in the closed conformation in which FANCI's ubiquitin, and therefore

225 FANCD2's ubiquitin too, are maximally protected. In support for this, the R1285Q mutant of FANCI,
226 which is predicted to disrupt the closed-on-DNA conformation of ubiquitinated ID2 complexes (Wang
227 *et al*, 2020; Rennie *et al*, 2020)(Fig. EV1), impairs both the DNA binding (Rennie *et al*, 2020) and the
228 I_{Ub}/$D2_{Ub}$ protection from USP1-UAF1-mediated deubiquitination (Wang *et al*, 2020). While closed-
229 conformation ubiquitinated ID2 complexes can exist in the absence of DNA, as previously shown for
230 $ID2_{Ub}$ (Rennie *et al*, 2020), such DNA-free complexes may be less stable, or conformationally more
231 flexible, without the avidity conferred by the interacting DNA. Therefore, they may be more amenable
232 to deubiquitination. Our biochemical assays indicate that FANCI ubiquitination further secures this
233 closed ID2 conformation. This is likely achieved through FANCI-ubiquitination effectively restricting
234 the conformational inclination of the USP1-UAF1-bound ID2 complex towards the open-state
235 conformation. Indeed, the structure of USP1-UAF1 complex bound to $ID2_{Ub}$-DNA revealed ID2
236 movements towards the open-state conformation, affecting not only FANCI helices in the region
237 where ubiquitin-conjugation occurs, but also, and most profoundly, the FANCD2 N-terminus involved
238 in interaction with FANCI's ubiquitin (Rennie *et al*, 2021). In ubiquitinated ID2 complexes, the ubiquitin
239 conjugated to FANCI is substantially more protected from deubiquitination than the ubiquitin
240 conjugated on FANCD2. To some extent, this may be due to USP1-UAF1 preferentially targeting
241 FANCD2, via USP1's N-terminal extension (Arkinson *et al*, 2018) and through UAF1-FANCI interactions
242 acting as a USP1-FANCD2 enzyme-substrate recruitment module (Rennie *et al*, 2021). Nevertheless,
243 the preferential targeting of FANCD2's ubiquitin over FANCI's ubiquitin may also be due to the latter
244 ubiquitin participating in more extensive interactions (than the former ubiquitin) with the other ID2
245 subunit (Fig. 4D-F)(Wang *et al*, 2020; Rennie *et al*, 2021). Further biochemical work, including
246 extensive mutagenesis of key ubiquitin-ID2 interfaces, is likely to uncover the reasons contributing to
247 $D2_{Ub}$ being preferentially targeted over I_{Ub} in ubiquitinated ID2 complexes.

248 In this work we provide a structural and biochemical basis for the *in vivo* interdependency in
249 FANCI and FANCD2 ubiquitination observed before (Smogorzewska *et al*, 2007). We further show that
250 DNA, along with FANCI ubiquitination is required for maintaining FANCD2 ubiquitination, while DNA
251 also protects from FANCI deubiquitination. Since DNA protects against both FANCI and FANCD2
252 deubiquitination, ubiquitinated ID2 complexes may need to be disengaged from DNA to be effectively
253 deubiquitinated. This could be achieved through the action of the DVC1-p97 ubiquitin segregase,
254 which has been shown to be responsible for removal of ID2 from sites of DNA damage, once ID2 has
255 been SUMOylated and subsequently polyubiquitinated on SUMO (Gibbs-Seymour *et al*, 2015).
256 Another possibility would be that ubiquitinated ID2 and/or USP1/UAF1 are modulated (by factors and
257 in ways that are yet unknown) for effective cleavage of the conjugated ubiquitins, in the presence of
258 DNA.

259

260 # Methods

261 **Protein expression and purification**

262 Protein constructs for protein expression were as before (Arkinson *et al*, 2018; Rennie *et al*,
263 2020). All proteins and ubiquitinated versions of FANCI and FANCD2 were produced as previously
264 described, in the absence of DNA, and ID2 complexes (with or without DNA) were subsequently
265 assembled *in vitro* (Arkinson *et al*, 2018; Rennie *et al*, 2020).

266

267 **DNA oligos**

All DNA oligos were purchased from IDT and consisted of perfectly complementary pairs for formation of double stranded DNA (dsDNA) molecules. Unlabelled DNA oligos (for 32 bp, 51 bp and 61 bp dsDNA formation) were PAGE-purified, whereas 5'-labelled with IRDye700 oligos (for infrared-labelled 32 bp dsDNA formation) were HPLC purified. Their 5' to 3' sequence is as following: 32 bp (labelled/unlabelled): CGATCGGTAACGTATGCTGAATCTGGTGCTGG and corresponding complementary sequence; 51 bp: CGTCGACTCTACATGAAGCTCGAAGCCATGAATTCAAATGACCTCTGATCA and corresponding complementary sequence; and 61 bp: TGATCAGAGGTCATTTGAATTCATGGCTTCGAGCTTCATGTAGAGTCGACGGTGCTGGGAT and corresponding complementary sequence.

Cryo-EM sample preparation, data collection and processing

Purified ubiquitinated His_6-V5-FANCI was mixed with purified FANCD2 at 1:1 molar ratio and exchanged into cryo-EM buffer (20 mM Tris, pH 8.0, 150 mM NaCl, 2 mM DTT) using a Bio-Spin P-30 column (Bio-Rad). The concentration of the recovered protein complex was estimated based on its absorbance at 280 nM. A PAGE-purified 61 base-pair dsDNA was then added to the protein complex at a 1:1 molar ratio. After a short equilibration at room temperature, 3.5 µl of the protein-DNA mix (7.6 µM) was loaded on Quantifoil 1.2/1.3 300 mesh grids, which had been previously glow discharged for 30 sec at 30 mA. Grids were blotted for 3 sec and vitrified in liquid ethane using a Vitrobot operating at 95% humidity at 18 °C. The frozen grids were subsequently imaged over two sessions on CRYO ARM 300 (JEOL) microscope (Scottish Centre for Macromolecular Imaging) using a DE64 detector. For the second session, the in-column omega filter was used, with a slit width of 30 eV. 45-frame movies (11,229 in total), with a calibrated pixel size of 1.023 Å, were collected in counting mode, using serialEM software (Mastronarde, 2005). Total electron dose was either 45.2 e/Å^2 or 46.8 e/Å^2 over 15.32 seconds. Movies were subsequently processed in cryoSPARC (v3.2) (Punjani *et al*, 2017) for particle-image extraction, 2D classification and construction/refinement of cryo-EM density maps, as detailed below. Each set of movies (from the two sessions) was processed separately for obtaining good particles. Following Patch motion correction, Patch CTF estimation and curation of resulting exposures, we obtained 10,178 dose-weighted motion-corrected images in total. Particles were first picked automatically using elliptical blobs having minimum and maximum diameters of 120 and 200 Å, respectively. All picked particles were extracted within a 320-pixel box. Following few rounds of 2D classification, particles forming good 2D classes were used for ab-initio 3D reconstruction (2-3 models) followed by heterogeneous refinement. To clear junk particles, the initial 3D classes were subjected to further rounds of heterogeneous refinement, using each time as an input particle-set the good 3D class output-particles of the previous hetero-refinement job. We then subjected the particles of the good 3D class to 2D classification to generate 2D templates for particle picking. The particle maximum diameter was set to 200 Å, in template-based particle picking. Template picking occurred twice with a different set of templates each time for both micrograph datasets. Removal of junk particles occurred with heterogeneous refinement, as before: all template-based extracted particle picks were subjected to multiple rounds of heterogeneous refinement, using one previously generated good, and 1-2 previously generated junk 3D classes. Multiple rounds of heterogeneous refinement was also applied to all particles extracted by blob-picking to enrich the good particle set. To further enrich the good particles of some 3D classes, ab-initio reconstruction (2-3 models) followed by heterogeneous refinement also occurred for these classes. After removal of any duplicate particles among the eight generated 3D classes (4 for each dataset) and another round of heterogeneous refinement, the 259,775 particles falling to the good 3D class were motion-corrected locally and re-extracted from the

314 micrographs. Following another round of heterogeneous refinement, the resulting good 3D class
315 (made of 206,669 particles) was low-pass filtered at 12, 18 and 30 Å. A final round of heterogeneous
316 refinement then occurred using the three low passed filtered volumes and a starting refinement
317 resolution set at 12 Å. The resulting highest resolution class (made of 139,601 particles) resulting from
318 the 12 Å filtered map, was both homogeneous and non-uniform refined. We then applied a local non-
319 uniform refinement (Punjani *et al*, 2020), using as inputs, the output volume of the non-uniform
320 refinement job, and the mask generated by the homogeneous refinement job. The generated map
321 had an overall resolution of 4.14 Å, determined by gold-standard FSC. A local resolution filtered map
322 was then obtained, by calculating the local resolution at 0.143 FSC threshold with an adaptive window
323 factor of eight. This map was used for model building, while a sharpened map produced with Phenix
324 (v1.19.2) auto-sharpen tool (Terwilliger *et al*, 2018) was also used to aide interpretation of higher
325 resolution features.

326

327 **Model building and visualization.**

328 Initially, the ubiquitin conjugated to FANCD2 in the $I_{Ub}D2_{Ub}$-DNA structure (PDB code:
329 6VAE)(Wang *et al*, 2020) was removed, and the remaining structure was fitted to the $I_{Ub}D2$-DNA map
330 using Chimera software. Model editing and building subsequently occurred in WinCoot (v0.9.4.1)
331 (Emsley *et al*, 2010), incorporating torsion, planar peptide, trans peptide and Ramachandran
332 restraints. More specifically: i) we corrected for peptide twists and mismatches to FANCI and FANCD2
333 human protein sequences (UniProt entries: Q9NVI1 and Q9BXW9, respectively); ii) we removed
334 regions corresponding to poor density - such as a large section of FANCI N-terminus (residues 1-171),
335 few FANCI/FANCD2 loops and a short stretch in one end (2 bp) of the 29bp dsDNA (closer to FANCD2
336 C-terminus); and iii) we filled some gaps in the structural model for which the cryo-EM density was
337 sufficiently good for modelling building. Then, we performed several rounds of, (global and local)
338 automated real-space refinement in Phenix (v1.19.2) (Afonine *et al*, 2018), followed by manual
339 refinement of problematic regions/residues in WinCoot. For automated refinement, protein/dsDNA
340 secondary structure, rotamer, Ramachadran, geometry and FANCI-Ub K523-G76 bond restrains were
341 enforced. Additionally, we applied a non-bonded weight of 2500 to restrict steric clashes. Cryo-EM
342 data and model refinement statistics are reported in Table 1. Maps and models were visualized in
343 PyMOL (The PyMOL Molecular Graphics System, Version 1.7.6.6 Schrödinger, LLC.), Chimera
344 (Pettersen *et al*, 2004), or ChimeraX (Goddard *et al*, 2018). Surface accessibility of non-conjugated
345 FANCI (K523) and FANCD2 (K561) target lysines in our $I_{Ub}D2$-DNA structure, and in ID2-DNA
346 (PDB:6VAA) and $ID2_{Ub}$ (PDB:6VAF) structures (Wang *et al*, 2020), was measured using the PDBePISA
347 tool (Krissinel & Henrick, 2007) at https://www.ebi.ac.uk/pdbe/pisa/.

348

349 **In vitro reactions**

350 FANCI-FANCD2 reactions occurred in 10 µl volume, using FLAG-tagged FANCD2 and/or His-V5-
351 tagged FANCI (Both N-terminally tagged). *In vitro* ubiquitination reactions were conducted at 30° C
352 with UBA1 (50 nM), UBE2Tv4 (2 µM), $FANCL^{109-375}$ (2 µM), ubiquitin (10 µM), ID2 (2 µM) and a 32 bp
353 dsDNA (3.6 µM), in 42 mM Tris-HCl pH 8, 140 mM NaCl, 5% Glycerol, 5 mM ATP, 5 mM $MgCl_2$ and
354 1mM DTT. *In vitro* deubiquitination reactions occurred at room temperature, with USP1-UAF1 (50 nM)
355 and ubiquitinated FANCI/ID2 (0.5 µM), in 50 mM Tris pH8, 100 mM NaCl, 5% Glycerol, 2 mM DTT.
356 Unless otherwise stated, deubiquitination reactions were performed in the presence of 2 µM dsDNA
357 (51 bp). Ubiquitination/deubiquitination reactions were terminated by addition of reducing LDS

358 sample buffer (to 1x final). After boiling for 3 min at 100° C, a fraction of these (amount corresponding
359 to approximately 0.5 pmoles of total ID2) were loaded on 4-12% Wedge-Well Tris-Glycine gels
360 (Thermo Fisher). Following SDS-PAGE, proteins were transferred to nitrocellulose membranes, using
361 an iBlot gel transfer device (Thermo Fisher). FLAG-FANCD2 and His_6-V5-FANCI were visualized, on
362 Odyssey CLx (LI-COR) infrared scanner, following western blotting with FANCD2 (sc-28194; Santa Cruz
363 Biotechnology) and V5 (66007.1-Ig; ProteinTech) primary antibodies, and corresponding infrared-dye-
364 conjugated secondary antibodies, as described before (Rennie *et al*, 2020).

365

366 **Protein Induced Fluorescence Enhancement assays**

367 These were performed using ubiquitinated or non-ubiquitinated His_6-V5-FANCI, non-
368 ubiquitinated His_6-FANCD2 and infrared (IRDye-700) labelled (on both strands) 32 bp DNA in
369 Fluorescence Buffer (20 mM Tris pH 8.0, 150 mM NaCl, 5% glycerol, 0.47 mg/ml BSA, 1 mM DTT). PIFE
370 assays were conducted as before (Rennie *et al*, 2020), but with the following modifications:
371 Ubiquitinated/non-ubiquitinated His_6-V5-FANCI was first diluted to 5 µM and then subjected to
372 several two-fold serial dilutions, whereas His_6-FANCD2 was mixed with labelled DNA to achieve a
373 working concentration of 5 µM FANCD2 and 250 nM DNA. Then 5 µl of this FANCD2-DNA mix was
374 mixed with 5 µl of each of the FANCI series of dilutions for final concentrations of: 125 nM DNA, 2.5
375 µM FANCD2 and 1.2 nM -2.5 µM of FANCI in Fluorescence Buffer. For assessing FANCD2's affinity to
376 dsDNA, His_6-FANCD2 was subjected to several two-fold serial dilutions and then each of this was mixed
377 with a constant concentration of labelled DNA to achieve final concentration of 125 nM DNA and 40
378 nM - 5 µM of FANCD2 in Fluorescence Buffer. Samples to be measured were transferred into premium
379 capillaries (NanoTemper Technologies). Measurements were performed at 22°C on a Monolith NT.115
380 instrument (NanoTemper Technologies) using the red channel, with laser power set to 20%.

381

382 **Quantification and statistical analysis**

383 For ubiquitination/deubiquitination experiments, the percentage FANCI/FANCD2
384 ubiquitination (induced-by-ubiquitination or residual-from-deubiquitination) at indicative time-
385 points, was calculated following quantification of ubiquitinated and non-ubiquitinated FANCI/FANCD2
386 bands from western blots, using LI-COR Image Studio Lite software (v5.2). All the percentage
387 ubiquitination values calculated for each complex/protein from multiple experiments were used in
388 fitting to either a one phase decay (deubiquitination experiments) or a one-phase association
389 (ubiquitination experiments) model, assuming same plateau for all proteins analysed. Assessment of
390 statistically significant changes was done using one-way ANOVA with Bonferroni correction.
391 Dissociation constants with associated uncertainties from Protein-Induced Fluorescence
392 Enhancement (PIFE) assays were determined by fitting baseline subtracted PIFE values to a one-site
393 binding model, as described before (Rennie *et al*, 2020). All data deriving from quantification of blots
394 and PIFE experiments were visualized and statistically analysed using GraphPad Prism software.

395

396 ## Data availability

397 The two half maps of the final cryo-EM $I_{Ub}D2$-DNA complex reconstruction, along with the locally
398 filtered and Phenix Autosharpen maps deriving from these, have been deposited to the Electron

Microscopy Data Bank with accession code EMD-14694. The atomic coordinates of the refined model have been deposited to the Protein Data Bank with accession code 7ZF1.

Author contribution

KL conceived, designed and performed the experiments, wrote the manuscript and made the figures. MLR conceived and designed PIFE experiments which he executed together with KL. MLR also helped KL with cryo-EM processing and structure modelling. KL, MLR, CA and VKC expressed and purified proteins. MC prepared grids. JS collected cryo-EM data. HW secured funding for the project. KL edited the manuscript with help from MLR, CA, JS and HW. All authors approved the final version of the manuscript.

Acknowledgments

Access to cryo-EM instrumentation was provided by the Scottish Centre for Macromolecular Imaging (SCMI), funded by the MRC (MC_PC_17135) and SFC (H17007). This work was supported by the European Research Council (ERC- 2015-CoG-681582 ICLUb) consolidator grant to HW.

References

Afonine P V., Poon BK, Read RJ, Sobolev O V., Terwilliger TC, Urzhumtsev A & Adams PD (2018) Real-space refinement in PHENIX for cryo-EM and crystallography. *urn:issn:2059-7983* 74: 531–544

Alcón P, Shakeel S, Chen ZA, Rappsilber J, Patel KJ & Passmore LA (2020) FANCD2–FANCI is a clamp stabilized on DNA by monoubiquitination of FANCD2 during DNA repair. *Nat Struct Mol Biol* 27: 240–248

Arkinson C, Chaugule VK, Toth R & Walden H (2018) Specificity for deubiquitination of monoubiquitinated FANCD2 is driven by the N-terminus of USP1. *Life Sci Alliance* 1: e201800162

Chaugule VK, Arkinson C, Rennie ML, Kamarainen O, Toth R & Walden H (2019) Allosteric mechanism for site-specific ubiquitination of FANCD2.

Emsley P, Lohkamp B, Scott WG & Cowtan K (2010) Features and development of Coot. *urn:issn:0907-4449* 66: 486–501

Garcia-Higuera I, Taniguchi T, Ganesan S, Meyn MS, Timmers C, Hejna J, Grompe M & D'Andrea AD (2001) Interaction of the Fanconi anemia proteins and BRCA1 in a common pathway. *Mol Cell* 7: 249–262

Gibbs-Seymour I, Oka Y, Rajendra E, Weinert BT, Passmore LA, Patel KJ, Olsen J V., Choudhary C, Bekker-Jensen S & Mailand N (2015) Ubiquitin-SUMO circuitry controls activated fanconi anemia ID complex dosage in response to DNA damage. *Mol Cell* 57: 150–164

Goddard TD, Huang CC, Meng EC, Pettersen EF, Couch GS, Morris JH & Ferrin TE (2018) UCSF ChimeraX: Meeting modern challenges in visualization and analysis. *Protein Sci* 27: 14–25

Kim JM, Parmar K, Huang M, Weinstock DM, Ruit CA, Kutok JL & D'Andrea AD (2009) Inactivation of Murine Usp1 Results in Genomic Instability and a Fanconi Anemia Phenotype. *Dev Cell* 16: 314–

438 320

439 Krissinel E & Henrick K (2007) Inference of Macromolecular Assemblies from Crystalline State. *J Mol*
440 *Biol* 372: 774–797

441 Lemonidis K, Arkinson C, Rennie ML & Walden H (2021) Mechanism, specificity, and function of
442 FANCD2-FANCI ubiquitination and deubiquitination. *FEBS J* doi:10.1111/febs.16077 [PREPRINT]

443 Longerich S, Kwon Y, Tsai MS, Hlaing AS, Kupfer GM & Sung P (2014) Regulation of FANCD2 and
444 FANCI monoubiquitination by their interaction and by DNA. *Nucleic Acids Res* 42: 5657–5670

445 Mastronarde DN (2005) Automated electron microscope tomography using robust prediction of
446 specimen movements. *J Struct Biol* 152: 36–51

447 Murai J, Yang K, Dejsuphong D, Hirota K, Takeda S & D'Andrea AD (2011) The USP1/UAF1 complex
448 promotes double-strand break repair through homologous recombination. *Mol Cell Biol* 31:
449 2462–9

450 Nalepa G & Clapp DW (2018) Fanconi anaemia and cancer: an intricate relationship. *Nat Rev Cancer*
451 18: 168–185

452 Oestergaard VH, Langevin F, Kuiken HJ, Pace P, Niedzwiedz W, Simpson LJ, Ohzeki M, Takata M, Sale
453 JE & Patel KJ (2007) Deubiquitination of FANCD2 Is Required for DNA Crosslink Repair. *Mol Cell*
454 28: 798–809

455 Pettersen EF, Goddard TD, Huang CC, Couch GS, Greenblatt DM, Meng EC & Ferrin TE (2004) UCSF
456 Chimera--a visualization system for exploratory research and analysis. *J Comput Chem* 25:
457 1605–1612

458 Punjani A, Rubinstein JL, Fleet DJ & Brubaker MA (2017) CryoSPARC: Algorithms for rapid
459 unsupervised cryo-EM structure determination. *Nat Methods* 14: 290–296

460 Punjani A, Zhang H & Fleet DJ (2020) Non-uniform refinement: adaptive regularization improves
461 single-particle cryo-EM reconstruction. *Nat Methods* 17: 1214–1221

462 Rajendra E, Oestergaard VH, Langevin F, Wang M, Dornan GL, Patel KJ & Passmore LA (2014) The
463 Genetic and Biochemical Basis of FANCD2 Monoubiquitination. *Mol Cell* 54: 858–869

464 Rennie ML, Arkinson C, Chaugule VK, Toth R & Walden H (2021) Structural basis of FANCD2
465 deubiquitination by USP1−UAF1. *Nat Struct Mol Biol* 28: 356–364

466 Rennie ML, Lemonidis K, Arkinson C, Chaugule VK, Clarke M, Streetley J, Spagnolo L & Walden H
467 (2020) Differential functions of FANCI and FANCD2 ubiquitination stabilize ID2 complex on
468 DNA. *EMBO Rep* 21: e50133

469 Sato K, Toda K, Ishiai M, Takata M & Kurumizaka H (2012) DNA robustly stimulates FANCD2
470 monoubiquitylation in the complex with FANCI. *Nucleic Acids Res* 40: 4553–4561

471 Smogorzewska A, Matsuoka S, Vinciguerra P, McDonald ER, Hurov KE, Luo J, Ballif BA, Gygi SP,
472 Hofmann K, D'Andrea AD, *et al* (2007) Identification of the FANCI Protein, a Monoubiquitinated
473 FANCD2 Paralog Required for DNA Repair. *Cell* 129: 289–301

474 Terwilliger TC, Sobolev O V., Afonine P V. & Adams PD (2018) Automated map sharpening by
475 maximization of detail and connectivity. *urn:issn:2059-7983* 74: 545–559

476 van Twest S, Murphy VJ, Hodson C, Tan W, Swuec P, O'Rourke JJ, Heierhorst J, Crismani W & Deans
477 AJ (2017) Mechanism of Ubiquitination and Deubiquitination in the Fanconi Anemia Pathway.
478 *Mol Cell* 65: 247–259

Wang R, Wang S, Dhar A, Peralta C & Nikola P (2020) DNA clamp function of the mono - ubiquitinated Fanconi Anemia FANCI - FANCD2 complex. *Nature* 580: 278–282

Wang S, Wang R, Peralta C, Yaseen A & Pavletich NP (2021) Structure of the FA core ubiquitin ligase closing the ID clamp on DNA. *Nat Struct Mol Biol* 28: 300–309

Tables and Figures

Table 1. Cryo-EM data collection and processing, and subsequent model building and refinement.

Data Collection and Processing		
Magnification		120,000x
Voltage (kV)		300
Electron exposure (e/Å2)		45.2 or 46.8
Pixel size (Å)		1.023
Defocus range (μm)		0.5-3.8
Symmetry imposed		C1
Initial number of images (automated picking)		7,376,277
Final particle images		139,601
Map resolution (Å) at FSC=0.143		4.1
Map resolution range (Å) at FSC=0.143		2.8-13.9
Refinement and Validation		
Initial model used (PDB code)		6VAE
Model resolution (Å)	Resolution at FSC=0.143	4.1
	Resolution at FSC=0.5	4.4
Model composition	Non-hydrogen atoms	19,458
	Protein residues	2,297
	DNA residues	54
All-Atom contacts	Clash score	3.24
Bonds RMSD	Bond Lengths (Å)	0.005
	Bond Angles (°)	0.81
Ramachandran plot	Favoured (%)	97.34
	Allowed (%)	2.66
	Outliers (%)	0
	Rama-Z score (RMSD)	0.76
Protein Geometry	MolProbity score	1.24
	Rotamer outliers (%)	0
	Cß outliers (%)	0
	Twisted peptides (%)	0
	CaBLAM outliers (%)	0.63
B-factors ($Å^2$)	Protein	127.49
	Nucleotide	306.24

Map-model correlation coefficients	CC_{MASK}	0.74
	CC_{BOX}	0.78

488

489

490

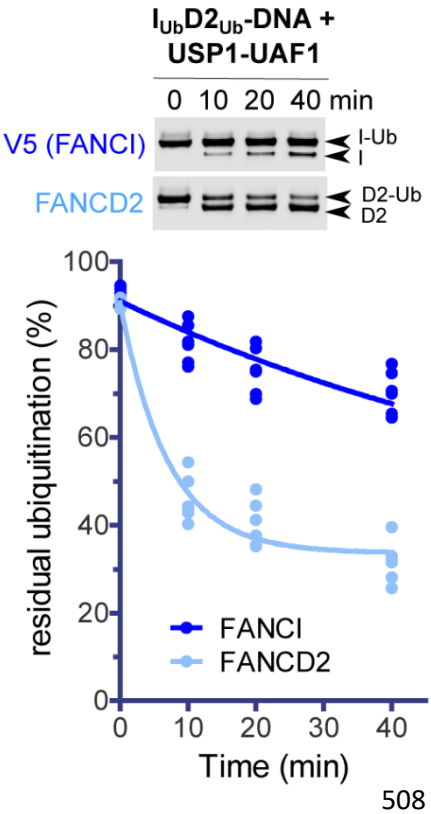

508

Fig. 1. FANCD2 deubiquitination progresses at much faster rate than FANCI deubiquitination.

$FANCI_{Ub}$-$FANCD2_{Ub}$-DNA complexes were assembled *in vitro*, and $FANCD2_{Ub}$ and V5-$FANCI_{Ub}$ deubiquitination by USP1-UAF1 (50 nM final) was monitored at room temperature in a time course: at indicative time-points aliquots of each reaction were removed and analysed by western blotting using FANCD2 and V5 antibodies. Experiment was repeated four times and FANCI/FANCD2 ubiquitination levels were calculated following quantification of ubiquitinated and non-ubiquitinated FANCI/FANCD2 bands from the blots. For each protein, all calculated values for all time-points were used for fitting to a one-phase decay model.

509

510

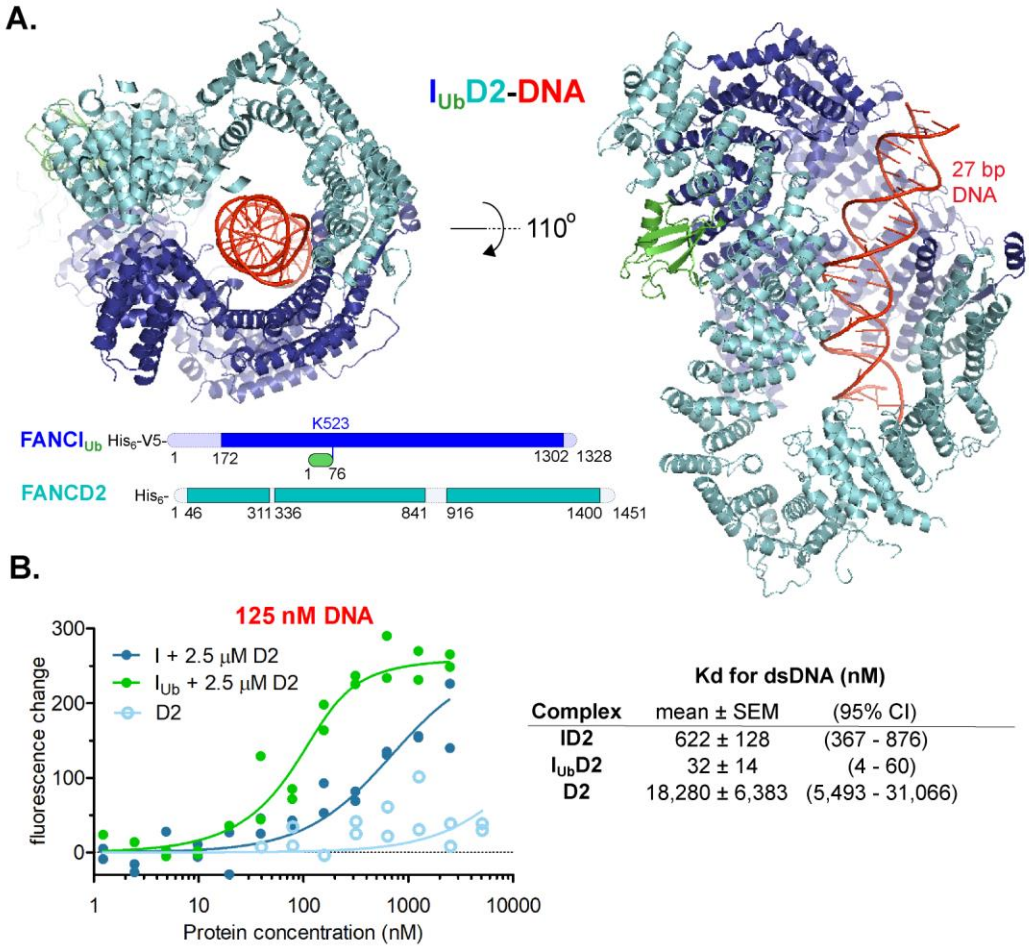

Fig. 2. FANCI$_{Ub}$-FANCD2 complex is a DNA clamp.

A. FANCI$_{Ub}$-FANCD2 (I$_{Ub}$D2) structure bound to double-stranded DNA. The structure was determined by cryo-EM, using a 4.1Å global resolution map. Two different views of the structure are shown. Unmodelled regions due to poor density that extend 20 amino-acid stretches are indicated at the bottom.

B. FANCI-ubiquitinated ID2 complex displays increased affinity to double-stranded DNA (dsDNA) compared to non-ubiquitinated ID2 complex. *Left*: Fluorescent changes of IRDye700-labeled 32 bp DNA (125 nM) when incubated with FANCD2 (D2; 2.5 µM) and increasing concentrations (ranging from 1.2 nM to 2.5 µM) of FANCI (I) or ubiquitinated FANCI (I$_{Ub}$). As a control, fluorescent changes of IRDye700-labelled DNA (125 nM) when incubated with increasing concentrations of FANCD2 (ranging from 40 nM to 5 µM) were monitored as well. For each protein/complex, the experiment was conducted twice and all data points from the two experiments were used for fitting of a one-site binding model. *Right*: Apparent ID2, I$_{Ub}$D2 and D2 Kd values (and associated uncertainties, all in nM) for dsDNA measured from model fitting.

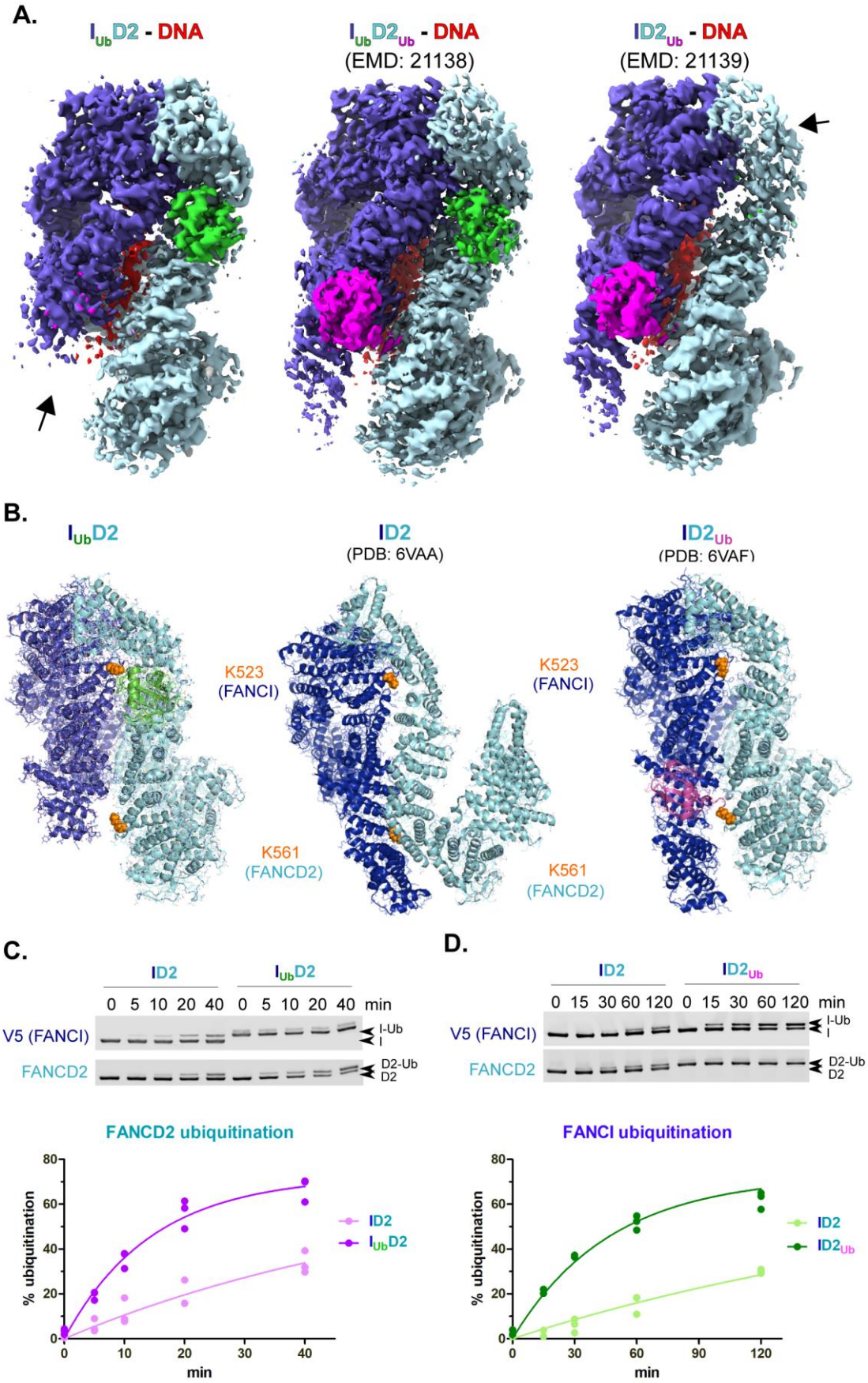

Fig. 3. Ubiquitination of either of the two ID2 subunits enhances ubiquitination of the other.

530 **A.** Comparison of cryo-EM density distribution among $I_{Ub}D2$-DNA (Phenix-auto-sharpened map),
531 $I_{Ub}D2_{Ub}$-DNA (EMD: 21138) and $ID2_{Ub}$-DNA (EMD: 21138) maps. $I_{Ub}D2$-DNA and $ID2_{Ub}$-DNA maps, as
532 well as $I_{Ub}D2_{Ub}$-DNA model (PDB: 6VAE) were aligned to $I_{Ub}D2_{Ub}$-DNA in ChimeraX. A different colour
533 was applied for each of the protein chains of $I_{Ub}D2_{Ub}$-DNA model (FANCI: slate blue, Ubiquitin-on-
534 FANCI: green, FANCD2: cyan, Ubiquitin-on-FANCD2: magenta), while DNA was coloured red. Then
535 each map was coloured according to nearby (within 6Å) residue colours. Contour levels were adjusted
536 ($I_{Ub}D2$-DNA: 6.21, $I_{Ub}D2_{Ub}$-DNA: 0.0194 and $ID2_{Ub}$-DNA: 0.0162) to achieve comparable volumes among
537 all displayed maps (ranging from 8.6 to 9.4 x 10^4 $Å^3$). Arrows indicate regions of poorer density (in
538 $I_{Ub}D2$-DNA and $ID2_{Ub}$-DNA maps) relative to other regions of the map, as well as to equivalent positions
539 in $ID2_{Ub}$-DNA map.

540 **B.** Structural comparison of relative accessibility of non-ubiquitinated FANCI-K523 and FANCD2-K561
541 in DNA-bound $I_{Ub}D2$, ID2 and $ID2_{Ub}$ complexes. The corresponding lysines are indicated as orange
542 spheres. For clarity DNA was removed from the structures. When only FANCI is ubiquitinated ($I_{Ub}D2$),
543 K561 of FANCD2 is fairly exposed for ubiquitination. When only FANCD2 is ubiquitinated ($ID2_{Ub}$), K523
544 of FANCI is fairly exposed for ubiquitination.

545 **C-D.** ID2 ubiquitination on FANCI results in increased rate of FANCD2 ubiquitination (B), whereas ID2
546 ubiquitination on FANCD2 results in increased rate of FANCI ubiquitination (C). Protein complexes
547 were assembled *in vitro* on ice in the presence of dsDNA (32 bp) and their *in vitro* ubiquitination at 30°
548 C was subsequently monitored in a time-course: at indicative time-points aliquots of the reaction were
549 removed and analysed by western blotting using FANCD2 and V5 antibodies (*Top*). For each protein
550 complex, data-points from three replicate experiments were used in fitting to a one-phase association
551 model (*Bottom*).

552

553

554

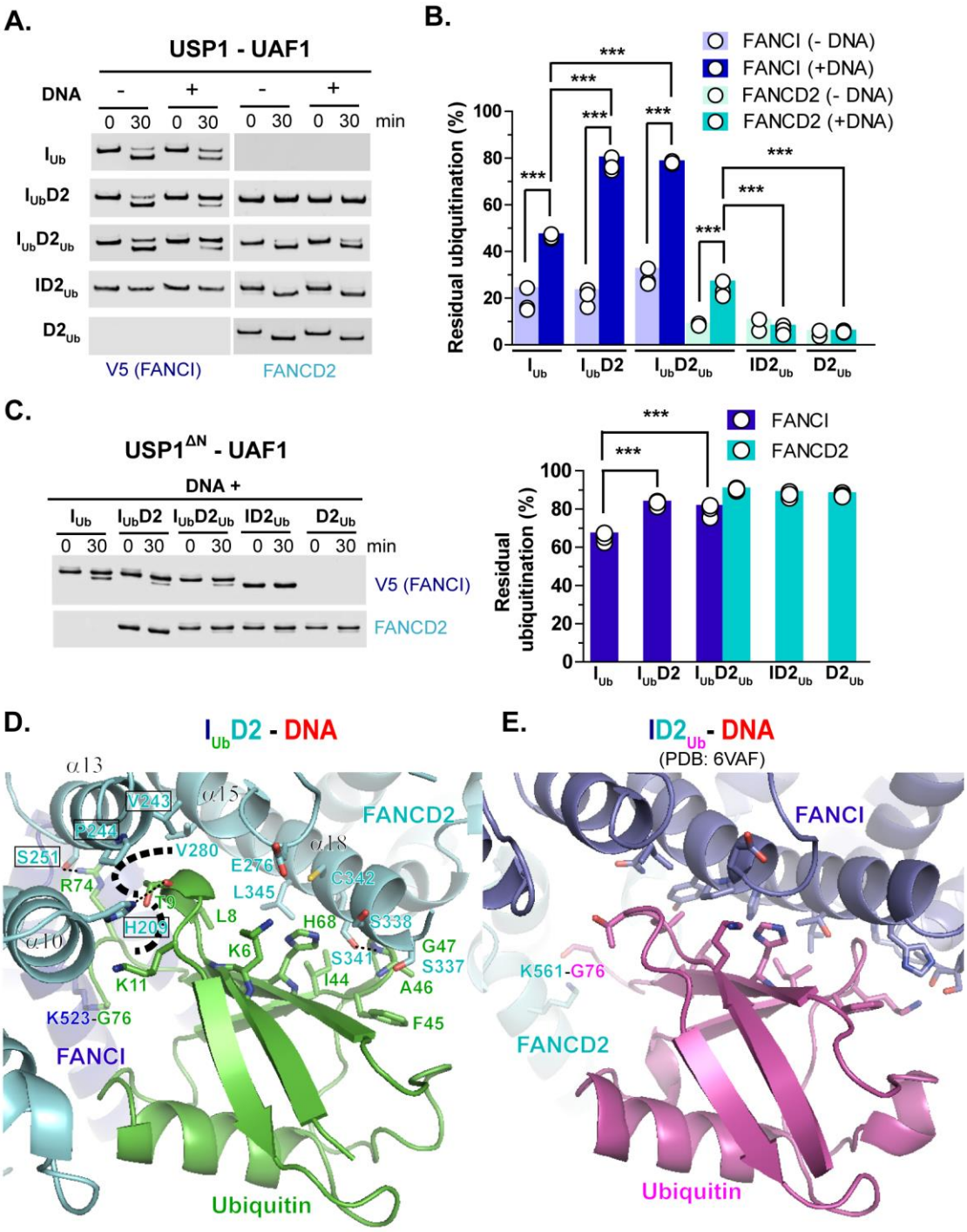

Fig. 4. DNA and FANCD2 protect against FANCI deubiquitination.

558 **A.** USP1-UAF1-mediated deubiquitination of V5-FANCI and FANCD2 was assessed in the absence or
559 presence of DNA (51 bp), when ubiquitinated versions of these proteins were in isolation (I_{Ub} and $D2_{Ub}$)
560 or within singly/doubly ubiquitinated ID2 complexes ($I_{Ub}D2$, $I_{Ub}D2_{Ub}$ and $ID2_{Ub}$). At indicated time-
561 points aliquots of each reaction were removed and analysed by western blotting using FANCD2 and
562 V5 antibodies.

563 **B.** Residual FANCI and FANCD2 ubiquitination following USP1-UAF1 treatment for 30 min at room
564 temperature. Experiments shown in A were performed in triplicate, apart from $ID2_{Ub}$ and $D2_{Ub}$
565 deubiquitination in the absence of DNA, which were performed twice (and were thus excluded from
566 statistical analysis). Replicate residual ubiquitination values and statistically significant changes (one-
567 way ANOVA test with Bonferroni correction) are shown. ***$p<0.001$.

568 **C.** Deletion of N-terminus (ΔN) of USP1 (residues 1-54) results in greatly reduced FANCD2
569 deubiquitination. Assays were performed in triplicate as in A, but all reactions contained DNA. *Left*:
570 Western blotting of reaction products at zero and 30 minutes using FANCD2 and V5 antibodies. *Right*:
571 Residual FANCI and FANCD2 ubiquitination following USP1-UAF1 treatment for 30 min. Replicate
572 residual ubiquitination values and statistically significant changes (one-way ANOVA test with
573 Bonferroni correction) are shown. ***$p<0.001$.

574 **D.** Ubiquitin-FANCD2 residue interactions in $I_{Ub}D2$-DNA structure. Dotted straight lines indicate
575 hydrogen bonding. The structure indicates predominantly hydrophobic interactions with two main
576 interfaces of FANCD2 with ubiquitin: one formed by FANCD2 α11 and α13 helices (interacting residues
577 highlighted in boxes) and residues T9 to K11 of ubiquitin, and another one formed by FANCD2 N-
578 terminal α18 helix region (residues S337 and S341) and residues F45 to G47 of ubiquitin. The former
579 interface (indicated with a thick dotted curve) does not correspond to an equivalent ubiquitin-FANCI
580 interface in $ID2_{Ub}$-DNA structure (D). Additional residues of ubiquitin and FANCD2 predicted to engage
581 in interactions (Wang *et al*, 2020) between the two proteins are also shown.

582 **E.** Ubiquitin-FANCI residue interactions in $ID2_{Ub}$-DNA structure (Wang *et al*, 2020). The structure was
583 aligned to the ubiquitin of $I_{Ub}D2$-DNA structure, so that both ubiquitins (in $I_{Ub}D2$-DNA and $ID2_{Ub}$-DNA,
584 shown in C and D, respectively) are in the same orientation for direct comparison of corresponding
585 interactions.

586 **F.** Clustal O multiple sequence alignment of human, mouse, rat, chicken, frog and zebrafish FANCD2
587 amino-acid sequences, focused on a region encompassing α11-13 helices of FANCD2 in human $I_{Ub}D2$-
588 DNA structure (helical regions shown on top). Identical residues among various species are highlighted
589 red, whereas identical/highly similar residues in positions showing 83% similarity are shown as red.
590 Residues of FANCD2 interacting with ubiquitin in $I_{Ub}D2$-DNA structure are indicated with blue circles.

591

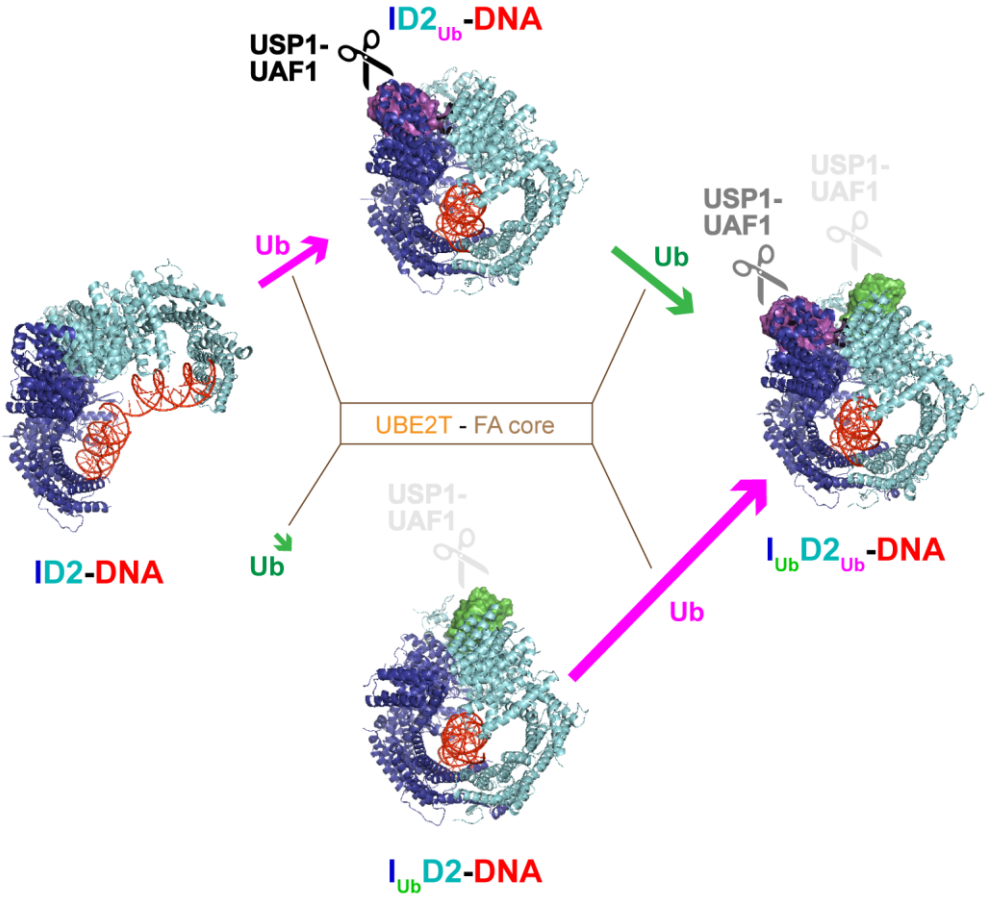

592

593 **Fig. 5. FANCI ubiquitination supports and maintains a di-mono-ubiquitinated ID2 state.**

594 Model explaining how the di-monoubiquitinated ID2 complex is generated and maintained. The
595 UBE2T ubiquitin conjugating enzyme partners with the FA core ubiquitin ligase for ubiquitination of
596 the DNA-bound FANCI-FANCD2 (ID2) complex. Of the two proteins subunits of the ID2 complex,
597 FANCD2 is preferentially targeted for ubiquitination. While the resulting complex ($ID2_{Ub}$-DNA) is
598 sensitive to USP1-UAF1 deubiquitination activity, it has a conformation that now favours FANCI
599 ubiquitination. Upon FANCI ubiquitination, the ubiquitin conjugated to FANCD2 gains some degree of
600 resistance towards USP1-UAF1-mediated deubiquitination ($I_{Ub}D2_{Ub}$-DNA complex). Nevertheless,
601 FANCD2's ubiquitin is preferentially targeted for deubiquitination in the $I_{Ub}D2_{Ub}$-DNA complex. Its
602 removal, though, is counteracted by very fast rates of FANCD2 ubiquitination (in the $I_{Ub}D2$-DNA
603 complex), which can (re-)establish the di-mono-ubiquitinated state ($I_{Ub}D2_{Ub}$-DNA). Since the ubiquitin-
604 on-FANCI is highly protected against deubiquitination in both $I_{Ub}D2$-DNA and $I_{Ub}D2_{Ub}$-DNA complexes,
605 reverting to a non-ubiquitinated ID2 state is highly disfavoured, once FANCI ubiquitination is
606 established. Arrow lengths are proportional to ubiquitination rates estimated in Fig 3C. ID2-DNA,
607 $ID2_{Ub}$-DNA and $I_{Ub}D2_{Ub}$-DNA structures shown correspond to PDB entries 6VAA, 6VAF and 6VAE,
608 respectively (Wang *et al*, 2020).

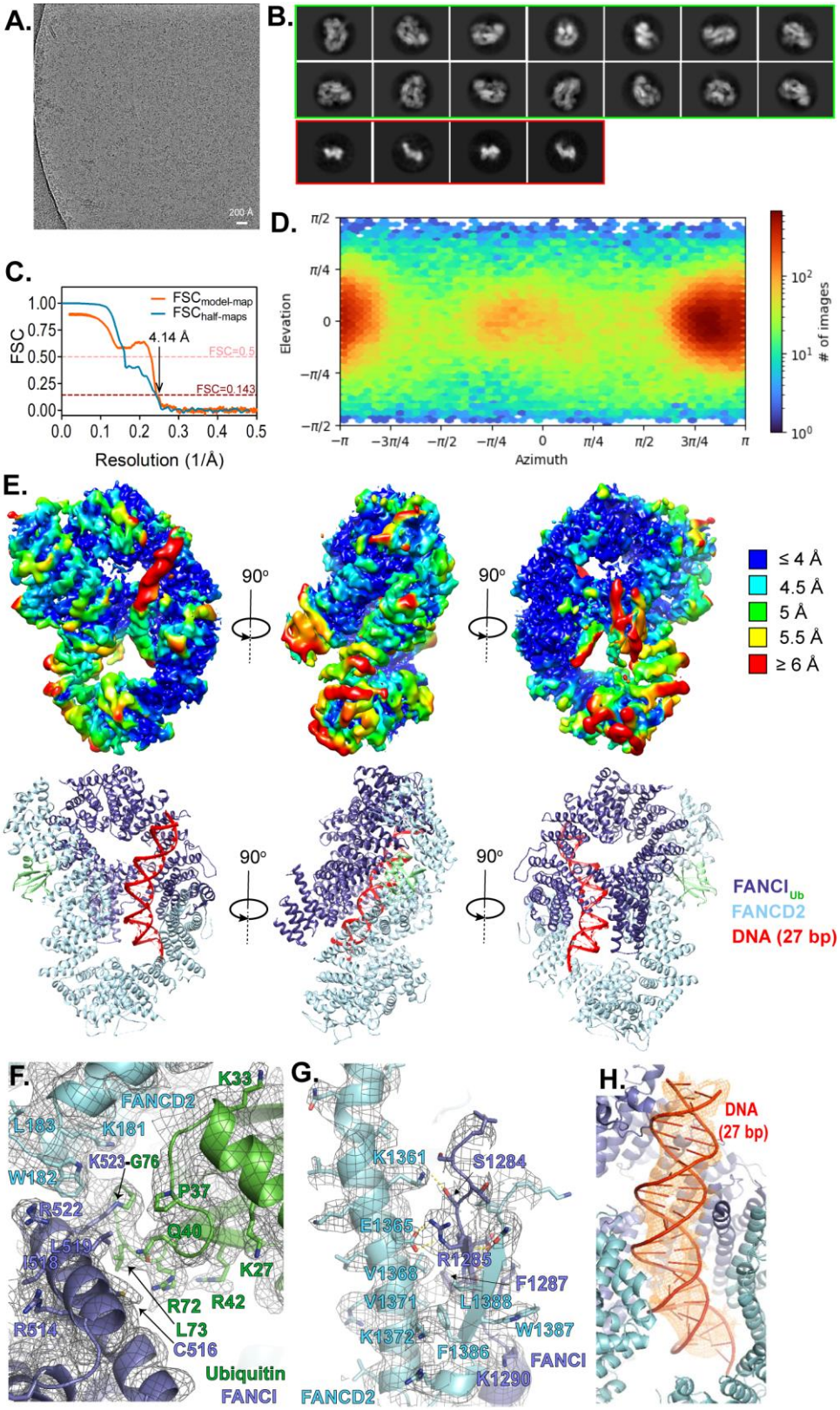

Fig. EV1. Cryo-EM analysis and structure modelling of $I_{Ub}D2$-DNA complex.

A. Example micrograph with scale bar.

612 **B.** Example 2D classes. Circular mask is 170Å in diameter. 2D classes surrounded by a green box
613 correspond to I_{Ub}D2-DNA complex particles, while smaller-sized 2D classes surrounded by a red box
614 likely correspond to monomeric I_{Ub}/D2 proteins.

615 **C.** Fourier Shell Correlation (FSC) curves: between the two half maps produced in the final local non-
616 uniform refinement (shown in blue) and between the refined model and final map (shown in orange).

617 **D.** Particle orientation (viewing direction distribution) in the final map. Total number of particles:
618 139,601.

619 **E.** *Top*: Locally filtered map coloured by local resolution, at three different angles. *Bottom*:
620 Corresponding structural model viewed under same orientations.

621 **F.** I_{Ub}D2-DNA structure with corresponding map density (locally filtered map), centred on the
622 isopeptide bond between K523 of FANCI and G76 of ubiquitin. Some well-resolved side-chains are
623 illustrated as sticks and indicated.

624 **G.** Interaction between FANCI and FANCD2 C-termini with corresponding map density (locally filtered
625 map). A beta-sheet consisting of a FANCI and a FANCD2 strand is formed (residues 1285-1289 of FANCI
626 and residues 1384-88 of FANCD2). This is held in place through hydrophobic and electrostatic
627 interactions with a FANCD2 helix (1351-1377 aa). Residues predicted to participate in such interactions
628 are shown as sticks and indicated. Selected side chains, for which there is good density are also shown
629 as sticks. For clarity, adjacent to that region elements of the I_{Ub}D2-DNA structure and map are
630 removed.

631 **H.** I_{Ub}D2-DNA structure centred on DNA. Density corresponding to the 27 bp modelled DNA is shown
632 as orange mesh. Colouring of structure is as in E-G.

633

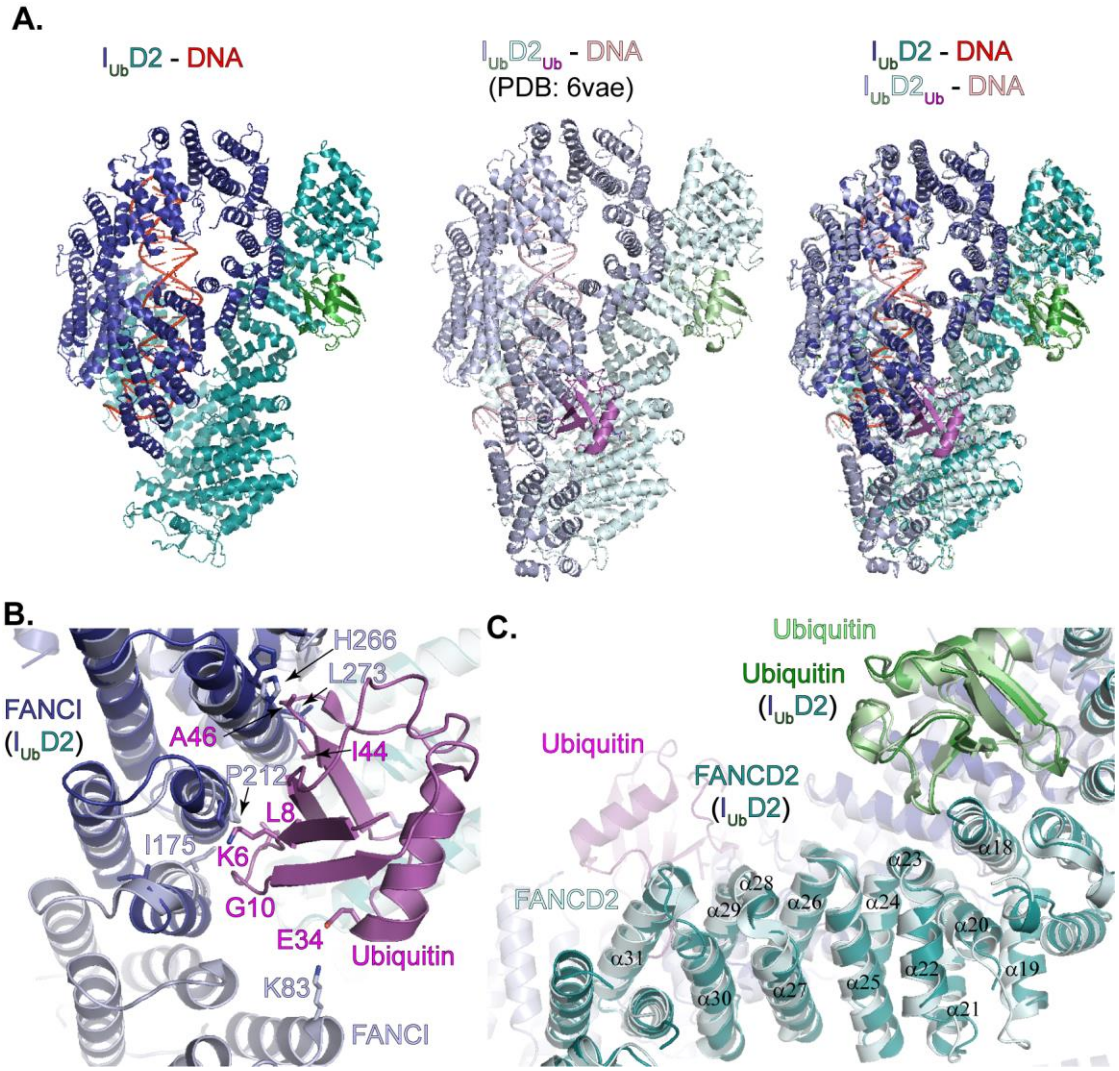

Fig. EV2. $I_{Ub}D2$-DNA and $I_{Ub}D2_{Ub}$-DNA structure comparison.

A. The lack of the FANCD2-conjugated ubiquitin in $I_{Ub}D2$-DNA structure is associated with a disorder in the 170 aa N-terminus of FANCI, when compared with $I_{Ub}D2_{Ub}$-DNA structure. The two structures were aligned in Pymol and visualized from the same angle, either on their own (*left* and *centre*), or together (*right*).

B. Helices and corresponding residues of FANCI involved in interaction with FANCD2's ubiquitin ($I_{Ub}D2_{Ub}$-DNA structure), are positioned differently when the ubiquitin is removed ($I_{Ub}D2$-DNA structure). Structures shown in A, were centred on FANCI N-terminus. Residues involved in ubiquitin-FANCI interactions are indicated and shown as sticks. The corresponding FANCI residues in $I_{Ub}D2$-DNA structure are also shown as sticks.

C. Removal of ubiquitin (magenta) from FANCD2 results in slight movements affecting several FANCD2 helices, from α31 (helix where ubiquitin is conjugated) up to α18. FANCD2 helices of $I_{Ub}D2$-DNA and $I_{Ub}D2_{Ub}$-DNA are better aligned towards the N-terminus of FANCD2, where interaction with the ubiquitin (green) conjugated to FANCI occurs (N-terminally to, and including α18 helix of FANCD2). The structures shown in A, were centred on the central part of FANCD2.